A New Approach for Geological Faults Detection

A.O. Cepero Díaz[1,2], V. Di Gesù[2], and C. Valenti[2,⋆]

[1] Departamento de Automática y Computación
Universidad Tecnológica de La Habana, Cuba

[2] Dipartimento di Matematica e Applicazioni
Università degli Studi di Palermo, Italy

Abstract. This paper will introduce a new approach, mainly based on wavelets transform and mathematical morphology, for the detection of geological faults in satellite and aerial photos. This can be useful for territorial analysis, digital cartography and the use of geographical information systems. The proposed method is fast enough and unsupervised. Different techniques will be compared and some examples on real data will be presented to indicate the applicability of these methods.

Keywords: geological faults, mathematical morphology, fuzzy morphology, wavelet image analysis.

1 Introduction

Geological systems for the analysis of multispectral images taken from satellites and airplanes usually require different experts and a lot of time. Actually, it is possible to spend months or even years in order to create an accurate map of a wide region. This information is embedded in a database which can be used, for instance, to create thematic maps and temporal reconstructions of the events (e.g. the evolution of the pollution, the type of the vegetation, the establishment of settlements, ...). Recently, a specific problem has been arisen by the research group of Dipartimento di Scienze della Terra in Siena, Italy, and it consists of the recognition of the outlines due to faults, usually perceived as darker zones. This is of great interest in several tasks such as cartography, underground or superficial characterization, the location of spring of water, the estimation of the stability of the slopes, and the driving in the extraction of stones. Traditionally, this duty is based on the identification of certain features (e.g. geometrical relations of the faults such as size, position and orientation) through campaigns and handmade analysis of the photos by using expensive hardware and software.

Although we have tested different techniques, such as the Hough transform, we will refer to three approaches which have given the most promising results. Here the suitability for high resolution image analysis of a well known wavelet algorithm is examined and its results are compared with those obtained by other methods already present in the literature. Tests on real images show that it is possible to analyze complex structures in a very fast way.

⋆ This work has been partially supported by ASI - Italian Space Agency - under grant I/R/117/00: "Tecniche ottimizzate di elaborazione, memorizzazione ed indicizzazione di immagini telerilevate".

O. Cepero Díaz A., Di Gesù V. and Valenti C. (2004).
A New Approach for Geological Faults Detection.
In *Proceedings of the 4th International Workshop on Pattern Recognition in Information Systems*, pages 216-221
DOI: 10.5220/0002686702160221

2 Standard methods

Mathematical morphology is a branch of digital image analysis which uses concepts of algebra and geometry [1, 2]. It has been successfully applied in the field of remote sensing to discriminate tree species [3], to segment soil maps [4], and to extract roads, rivers, villages [5].

2.1 Standard mathematical morphology

A fast algorithm for directional morphological filtering to extract long thin objects in satellite images has been introduced in [6]. In our first technique, we have implemented both the erosion ε and the dilation δ of the input image I:

$$\varepsilon_X(I)(\underline{p}) = \min_{\underline{q} \in X} I(\underline{p} + \underline{q}) \quad \text{and} \quad \delta_X(I)(\underline{p}) = \max_{\underline{q} \in X} I(\underline{p} + \underline{q})$$

where X represents, along a variety angles, a binary bar with generic length and width. In practice, the erosion (dilation) is defined on the grey level image I by computing the local minimum (maximum) around each point $\underline{p}$. The exact shape of this neighborhood is easily defined by that of the structuring element X. Assuming a fault as the union of consecutive segments, darker than the background, we have enhanced it by applying the opening operator $\gamma = \delta\varepsilon$. We must do it a lot of times along different orientations to highlight all the faults and the final map will contain the local maxima among all opened images. An example for 16 angles and bars of 15×3 pixels is shown in Figures 1*a*,*b*.

2.2 Fuzzy mathematical morphology

In order to apply fuzzy mathematical morphology [7, 8], we transform both the image I and the non-flat structuring element X in fuzzy sets and reinterpret their intensity values as a grade of membership. All usual mathematical morphology operators can be generalized and it is possible to extend to grey level images some inequalities that hold for binary images in the case of standard mathematical morphology. Here, we will recall only the definition of correlation:

$$\rho_{\underline{p}} = \frac{1 + \sum_{\underline{q} \in X} (X(\underline{q}) - \mu_X) \cdot (I(\underline{p} + \underline{q}) - \mu_{\underline{p}})}{2|\sigma_X \sigma_{I_{\underline{p}}}|}$$

where μ_X (σ_X) and $\mu_{I_{\underline{p}}}$ ($\sigma_{I_{\underline{p}}}$) are the mean (standard deviation) values of X and the sub-image of I, with the same shape and size of X and centered in $\underline{p}$.

Best correlation (i.e. $\rho = 1$) is obtained when the considered sub-image is exactly like X. This definition of correlation exalts both dark and bright outlines and therefore we have to select the former ones by computing their average luminosity. As for the morphological opening, we then calculate the image of local maxima. Figure 1*c* shows the map of matching degree obtained by rotating along 16 directions a Gaussian structuring element of 21×9 pixels.

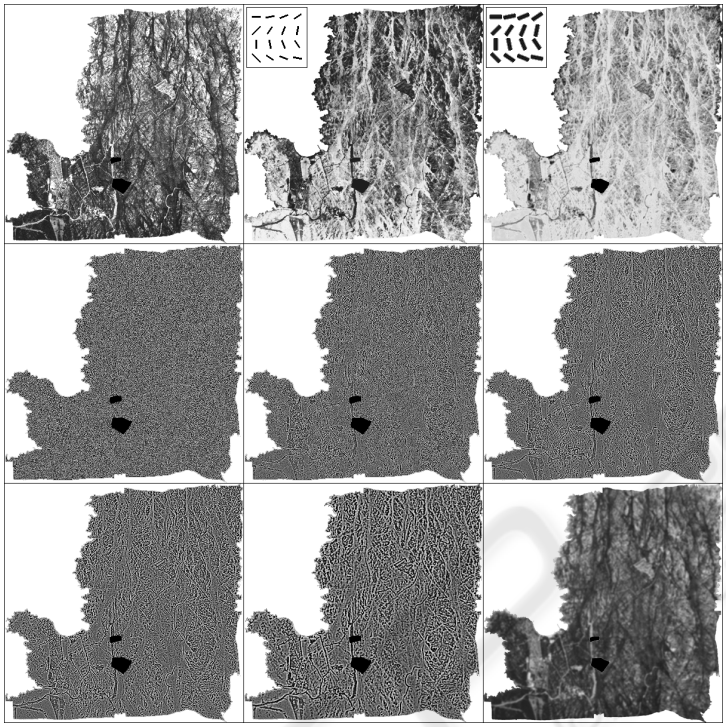

Fig. 1. *a*: aerial photo (4096×4096) of the Caprera Isle. The black zones corresponds to military sites. *b*: mathematical morphology erosion. *c*: fuzzy correlation. The structuring elements, not on scale, are superimposed on (*b,c*). *d–h, i*: wavelet and residual planes by the *à trous* algorithm. All histograms have been stretched for clarity.

3 Analysis based on wavelets transform

Wavelets provide an alternative approach to signal processing and constitute a link between mathematics, physics and electrical engineering. The so called *à trous* procedure [9] maps the input signal to its coefficients with respect to a basis of wavelet functions, constructed by dilation and translation of a *mother wavelet* function [10]. The underlying idea is simple and the process, sketched as follows, is very fast. At step i, get a smoother version c_i of I by convolving with a high-pass filter and compute the wavelet coefficients w_i by a low-pass filter:

$$c_0(\underline{p}) = I(\underline{p}), \quad c_i(\underline{p}) = \left\langle c_{i-1}(\underline{p} + 2^{i-1}\underline{q}),\ h(\underline{q}) \right\rangle, \quad \text{and} \quad w_i(\underline{p}) = c_{i-1}(\underline{p}) - c_i(\underline{p}).$$

In practice, both c_i and w_i have the same size of I. Figures 1*d–i* show the application of the *à trous* algorithm. The planes w_1 and w_p contain the highest and lowest frequencies, that is the finest and coarsest details of I, respectively. When the desired resolution j has been reached, the original image can be expressed as the sum of all w_i and the final smoothed approximation c_j:

$$I(\underline{p}) = \sum_{i=1}^{j} w_i(\underline{p}) + c_j(\underline{p}).$$

The kernel has been obtained via a B_1-*spline* function:

$$h = \frac{1}{16}\begin{pmatrix} 1 & 2 & 1 \\ 2 & 4 & 2 \\ 1 & 2 & 1 \end{pmatrix}.$$

This function has been selected thanks to the fact that it is compact (reducing the boundary artifacts at block edges), isotropic (not privileging any direction), and limited to 9 elements, whatever the level i of the scale is (an average personal computer can calculate each plane w_i of a high resolution photo in about 5 seconds). Moreover, other classical scaling functions such as B_3-*spline*, $Meyer$ or $Daubechies_4$ [11, 12] seem to return too smoothed wavelet images.

4 Experiments and comparison of the methods

After applying the above methods we binarize their results by just setting a threshold value equal to the average luminosity of each single image. This is valid for all three approaches but, of course, we select the right wavelet plane according to *a priori* knowledge of the faults in input image. To compare the output of each method we have considered only the plane w_4.

In order to put better in evidence the faults we calculate the skeleton of the selected binary images [13]. Usually the corresponding graph is too dense and we have to prune it. In particular, many of its cycles are due to small bright spots inside the faults of the input image. We have verified that, before of the skeletonization, it is sufficient to eliminate in the binary images all black *4-connected* components which are too small (area less than 35 pixels in the case of morphology or area less then 150 pixels in the case of the wavelet transform) and/or too dark in the original photo (average luminosity less than 25%). Please note that a white zone in the binary images correspond to a possible fault in the original photo. Finally, we remove all arcs (considered as *8-connected* objects) that are isolated and too small (length less than 20 pixels). Figures 2 illustrates the main steps of the pruning procedure. We want to stress that we have carried out an extensive simulation to determine a suitable set of parameters needed to threshold the auxiliary images or to prune the graphs.

We have analyzed high resolution photos, provided by Dipartimento di Scienze della Terra in Siena, Italy, [14] or freely downloaded from the web [15, 16]. The results obtained by the pipeline of methods above described have been compared with those carried out by photo-interpreters. See Figure 3 for the output relative to Figure 2*a*. To verify the robustness of the whole procedure we have also introduced a range of uniform *salt and pepper* noise. A successive convolution with a Gaussian filter was enough to disperse the influence of the wrong pixels.

Morphological opening is simple and fast, thanks to the use of temporary look-up tables. In practice, filtering along each orientation can be applied in linear time, so allowing to reach a high angular resolution. We have observed that pairs of close and parallel faults are often misinterpreted as one bigger line.

Fuzzy correlation makes use of floating point operations and has a time complexity proportional to the size of the structuring element. As for mathematical morphology, the choice of the structuring element is very important and we have defined many of them to correctly detect faults with different shapes and dimensions. Nevertheless, it has correctly detected most of the faults.

A faster execution and a higher accuracy have been achieved by the wavelet transform. Its multiresolution support natively puts in evidence structures with different sizes and, despite the other two previous approaches, the skeleton is smooth. Moreover, no custom kernel is needed to analyze faults with particular slopes, which can be extracted during the pruning phase.

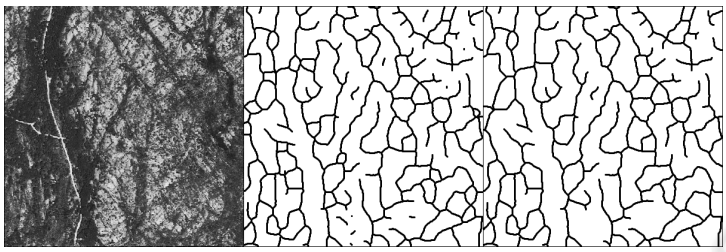

Fig. 2. *a*: a detail (400 × 400) of Figure 1*a*. *b,c*: raw and cleaned skeletons of w_4.

5 Conclusions and perspectives

A new unsupervised detector of geological faults in high resolution photos taken from satellite and airplane has been presented. This can be useful in solving several tasks such as digital cartography, underground or superficial characterization, geographical information interpretation. At present, geologists have to analyze almost by hand a huge amount data, to be integrated with information obtained through campaigns. The whole procedure is expensive and very slow.

We have compared three different methods based on mathematical morphology, fuzzy morphology and wavelet analysis. The first two methods process the input image through structuring elements with a variety of sizes and orientations and have returned similar outputs. Their accuracy strictly depends on the choice of the shape of the structuring element and are sensitive to the change of luminosity. For example, they usually tend to cross the streets, when partially occluded by trees. The latter approach has shown to be fast and accurate when putting in evidence both fine and coarse outlines. It is based on a sequence of convolutions with a compact kernel. Moreover, it does not privilege faults with a specific direction and therefore there is no need to consider a set of orientations.

A skeletonization let us reduce the size of the binarized regions of interest, obtained by any one of the above methods. The new image can be considered as a graph and its arcs represent pieces of faults. We have demonstrated that pruning the graph enhances the final result though more efforts can still be made in order to make the shape of the graph smoother by computing, for example, the minimum spanning tree and regularization formulas.

The efficiency of the detector has been verified with a database of real images and we have introduced *salt and pepper* noise to test the robustness of the methods. We have roughly estimated the running time, showing that these algorithms are fast enough. Moreover, it should be relatively easy to embed them on the actual software, such as Imagine and ArcView, already employed by geologists.

Acknowledgements

We wish to thank the group of Dipartimento di Scienze della Terra in Siena, led by Prof. Carmignani, and especially Dr. Disperati for providing the input data.

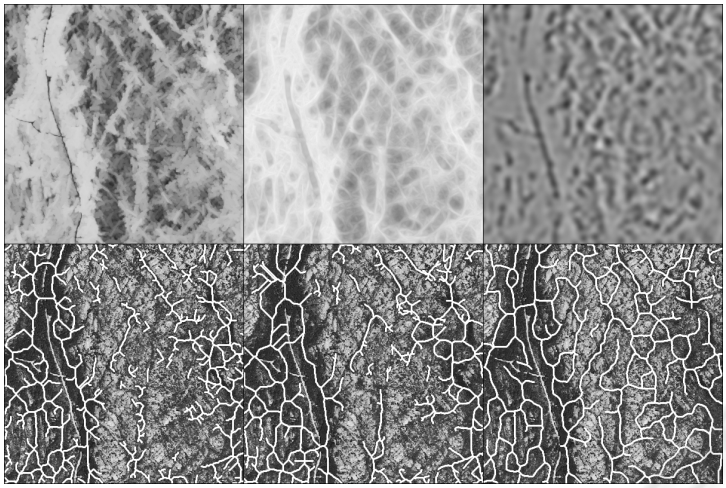

Fig. 3. *a*: morphological opening. *b*: fuzzy correlation. *c*: w_4 of the *à trous* algorithm. *g–i*: cleaned skeletons of (*a–c*) superimposed on Figure 2*a*.

References

1. Serra J., *Image analysis and mathematical morphology*, Academic Press (1982).
2. Soille P., *Morphological Image Analysis*, Springer-Verlag, Second Edition (2003).
3. Zheng X., Gong P. and Strome M., *Characterizing spatial structure of tree canopy using colour photographs and mathematical morphology*, Canadian Journal of Remote Sensing, Vol.21, No.4 (1995) 420–428.
4. Ansoult M., Soille P. and Loodts J., *Mathematical morphology: a tool for automated GIS data acquisition from scanned thematic maps*, Photogrammetric Engineering and Remote Sensing, Vol.56, No.9 (1990) 1263–1271.
5. Destival I., *Mathematical morphology applied to remote sensing*, Acta Astronautica, Vol.13, No.6-7 (1986) 371–385.
6. Soille P. and Talbot H., *Directional Morphological Filtering*, IEEE Transactions on Pattern Analysis and Machine Intelligence, Vol.23, No.11 (2001) 1313–1329.
7. Di Gesù V., Maccarone M.C. and Tripiciano M., *Mathematical Morphology Based on Fuzzy Operators*, Fuzzy Logic, Kluwer Academic Publishers (1993) 477–486.
8. Maccarone M.C., *Fuzzy mathematical morphology: concepts and applications*, Vision Modeling and Information Coding, Vistas in Astronomy, Vol.40, No.4 (1996) 469–477.
9. Holschneider M., Kronland-Martinet R., Morlet J. and Tchamitchian Ph., *The à trous Algorith*m, CPT-88/P.2215, Berlin (1988) 1–22.
10. Grossmann A. and Morlet J., *Decomposition of Hardy functions into square integrable wavelets of constant shape*, SIAM J. Math. Anal., Vol.15, No.4 (1984) 723–736.
11. Daubechies I., *Ten Lectures on Wavelets*, CBMS-NSF Regional Conference Series on Applied Mathematics, Vol.61, Soc. for Industrial and Applied Mathematics (1992).
12. Graps A., *An Introduction to Wavelets*, IEEE Computational Science and Engineering, Vol.2, No.2 (1995).
13. Klette R. and Zamperoni P., *Handbook of Image Processing Operators*, John Wiley & Sons (1996).
14. *Memorie descrittive della Carta Geologica d'Italia*, Istituto Poligrafico e Zecca dello Stato, Vol.60, (2001).
15. The SIRIUS Spot Image catalogue, `http://sirius.spotimage.fr`
16. The MODIS web, `http://modis.gsfc.nasa.gov`